Modal active control of Chinese gongs

Marguerite Jossic[a)]
Sorbonne Universités, UPMC Univ Paris 06, CNRS, UMR 7190 Institut Jean Le Rond d'Alembert, F-75005 Paris, France

Adrien Mamou-Mani
Sorbonne Universités, UPMC Univ Paris 06, IRCAM, CNRS, UMR 9912 Science and Technology of Music and Sound lab, F-75004, Paris, France

Baptiste Chomette
Sorbonne Universités, UPMC Univ Paris 06, CNRS, UMR 7190 Institut Jean Le Rond d'Alembert, F-75005 Paris, France

David Roze
Sorbonne Universités, UPMC Univ Paris 06, IRCAM, CNRS, UMR 9912 Science and Technology of Music and Sound lab F-75004, Paris, France

François Ollivier and Christophe Josserand
Sorbonne Universités, UPMC Univ Paris 06, CNRS, UMR 7190 Institut Jean Le Rond d'Alembert, F-75005 Paris, France

(Received 29 October 2016; revised 16 May 2017; accepted 21 May 2017; published online 20 June 2017)

Instruments that belong to the gong family exhibit nonlinear dynamics at large amplitudes of vibration. In the specific case of the *xiaoluo* gong, this nonlinear behavior results in a pitch glide of several modes of the instrument in addition to harmonic distortion and internal resonances. This study applies a linear modal active control to a *xiaoluo* gong in an attempt to change its sound properties. First, a modal damping control of the fundamental mode based on a linear identification and a state space controller is applied in the small amplitude regime (no pitch glide). Results indicate that modal control influences not only the controlled mode but also the frequency components involved in distortion or internal resonance phenomena. Second, a modal damping control is performed in the large amplitude regime (in the presence of pitch glide). Results show that modal control does not affect the pitch glide. However, the controller becomes effective at a time trigger which is related to the instantaneous frequency. © *2017 Acoustical Society of America*.
[http://dx.doi.org/10.1121/1.4985108]

[TRM] Pages: 4567–4578

I. INTRODUCTION

Active control of musical instruments is of great interest for improving instrument quality and enhancing musical performance.[1,2] Active control uses a feedback loop consisting of a controller and a set of actuators and sensors added to the vibrating part of the instrument. Among the variety of existing techniques, modal active control, based on the control of identified vibration modes, has proven to be promising for controlling the sound of instruments. The significant relation between modal parameters and instrument's sound[3,4] allows this control technique to explore new and interesting directions for the control of vibration characteristics and, therefore, the sound of the instrument. Since modal control relies on linear models of the structures, it is particularly suited to instruments that maintain a linear behavior in regular playing conditions. The studies of Benacchio and coworkers[5,6] and Meurisse *et al.*[7] are successful examples of experimental modal control applied to a guitar soundboard and a simplified clarinet, respectively.

However, instrument resonators may present a nonlinear response in normal playing conditions.[4] This is especially true for percussions. In the case of gongs and cymbals, vibration amplitudes on the order of the plate thickness lead to geometrical nonlinearities in the instrument's dynamic behavior.[8] In particular, typical plate vibration phenomena, such as hysteresis, distortion, or chaos can be observed.[9]

When considering gongs, two main families can be identified according to the intensity of the nonlinear effects in the instrument's behavior. The first family contains the Chinese tam-tam and exhibits highly nonlinear vibrations and chaotic behavior.[10,11] The second family is referred to weakly nonlinear percussions and includes Chinese opera gongs which exhibit contrary pitch glides. In the current study our attention focuses on Chinese opera gongs in order to avoid chaotic behavior like those encountered in Chinese tam-tams. The pitch glide of Chinese opera gongs depends on the curvature and thickness of their central area.[12] The balance between these two parameters determines the hardening or softening behavior of the instrument.[8,13] The larger

[a)]Also at: Sorbonne Universités, UPMC Univ Paris 06, IRCAM, CNRS, UMR 9912 Sciences and Technology of Music and Sound Lab, F-75004, Paris, France. Electronic mail: marguerite.jossic@upmc.fr

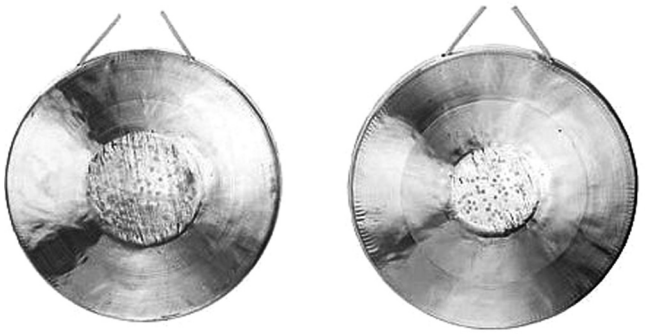

FIG. 1. Two different Chinese opera gongs: the *xiaoluo*, displaying a convex central section (left) and the *daluo*, displaying a flat central area (right).

Chinese opera gongs, called *daluo* (Fig. 1, right), present a flat central section and exhibit a hardening behavior associated with a downward pitch glide; smaller gongs, called *xiaoluo* (Fig. 1, left), present a convex central section and exhibit a softening behavior resulting in an upward pitch glide.

Linear models are expected to be inadequate to predict the nonlinear behavior of gongs. In consequence, the relevance of using linear control techniques to control such instruments is an open question. On the other hand, nonlinear control is often difficult to handle as it requires the identification of nonlinear models[14] which are so far incomplete for systems with global nonlinearities like gongs. In this context, it may be interesting to apply linear control to nonlinear instruments to evaluate the relevance of such a technique for the control of significant nonlinear phenomena inherent to these instruments. Such control is of particular interest in the case of instruments for which nonlinear phenomena—e.g., pitch glides in Chinese gongs, or internal resonances in steel-pan[15]—significantly influence the sound timbre.

In the present study, we aim to apply the simplified framework of modal control[16] applied to the *xiaoluo* gong. In particular, we will infer the performances and limits of modal control on phenomena induced by geometrical nonlinearities. For this purpose, our control experiments focus on modal damping control, therefore excluding frequency control. The modal control is specifically applied to the fundamental mode in order to properly separate the origin of nonlinear phenomena.

In order to explore the whole range of possible responses, two distinct vibration regimes will be distinguished: In the "small amplitude regime," no pitch glide occurs and the main nonlinear phenomena pertain to harmonic distorsions and internal resonances. In the "large amplitude regime," these nonlinear phenomena also occur but a pitch glide of one or several modes is additionally observed.

The present paper is organized as follows. Section II provides a brief summary of the nonlinear dynamics of gongs and modal active control theory. Then, the experimental set-up is presented in Sec. III. The results are reported in Sec. IV, both for the small and large amplitude regimes. Finally, the performances and limitations of modal control are discussed in Sec. V. Some conclusions and perspectives are presented in Sec. VI.

II. THEORETICAL BACKGROUND

A. Nonlinear behavior of Chinese opera gongs

Chinese gongs can be considered thin structures which exhibit geometrical nonlinearities when subjected to large amplitude flexural vibrations.[10] In such cases, the relationship between displacements and deformations can no longer be considered as linear, leading to so-called geometrical nonlinearities in dynamical equations that are responsible for the appearance of specific phenomena.[9] In the case of the *xiaoluo*, these nonlinear phenomena correspond to harmonic distortion, internal resonances, and pitch glides. The following paragraph underlines qualitative rather than quantitative features of Chinese gongs; for more details, the reader can refer to Refs. 9 and 17.

An illustrative and simple example of the nonlinear behavior of complex structures like gongs is given by Thomas *et al.*[8] These authors provide an analogy between these structures and simple one-degree-of-freedom rod systems which all exhibit nonlinear stretching for large magnitude of the transverse displacement. In particular, for a one-degree-of-freedom system with geometrical nonlinearities, the equation of motion reduces to a Duffing equation with an additional quadratic term. The nonlinear terms of such equation are responsible for the appearance of two nonlinear phenomena in the gong's response: harmonic distortion and pitch glide.

Harmonic distortion refers to frequency components with pulsations that are multiples of the oscillator modal pulsation ω_0.[9] In the case of the *xiaoluo*, these harmonics emerge from very small vibration amplitudes. An example of quadratic and cubic distortion of the fundamental mode ($\omega_0 \sim 451$ Hz) is shown in Fig. 2(a) (horizontal green arrows).

Pitch glide corresponds to an amplitude-frequency dependence of the oscillations. Assuming that the nonlinear terms of the Duffing equation are small in comparison to the linear terms, multiple scale methods[9,18] can be applied to establish the relationship between the pulsation ω of the vibration and the amplitude A of the displacement at frequency ω,

$$\omega = \omega_0(1 + CA^2), \tag{1}$$

where $C \in \mathbb{R}$. The sign of coefficient C controls the trend of the nonlinearity, and thus the pitch glide direction of Chinese gongs: for $C > 0$ the gong has hardening behavior, whereas for $C < 0$ it has a softening behavior. The complete expression of C is reported in Ref. 8. This frequency-amplitude dependence of the *xiaoluo* is observed for several modes in the large amplitude regime [see Fig. 2(b)]: the fundamental mode exhibits an upward pitch glide from 370 to 450 Hz highlighting a softening behavior.

The above discussion is valid for a one-degree-of-freedom system. In a multiple degree-of-freedom system, internal resonances may occur when two or more natural frequencies are commensurable or near commensurable.[9] Such resonances lead to strong coupling and energy exchanges between the corresponding linear modes. The resonance relationships

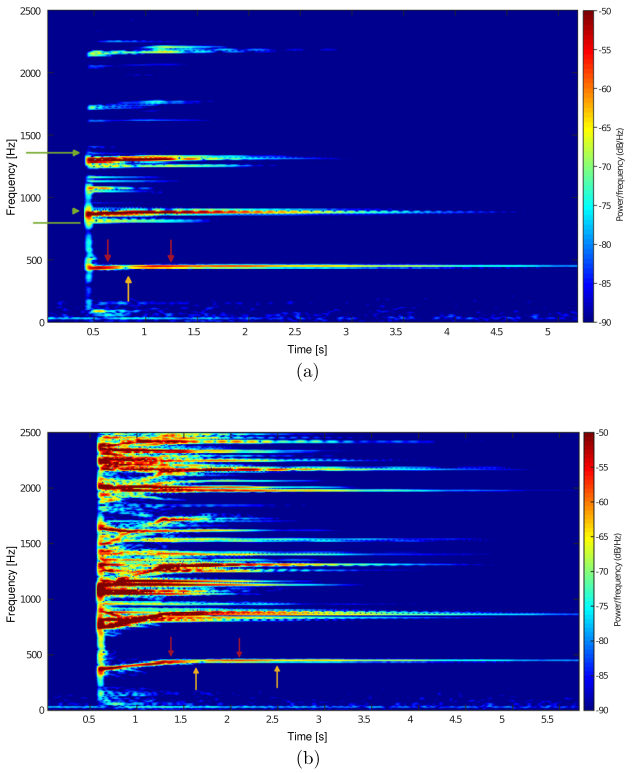

FIG. 2. (Color online) Spectrograms of the sound of the *xiaoluo* in (a) the small amplitude regime (no pitch glide) and (b) the large amplitude regime (with pitch glide). In both panels, alternating maxima (marked by downwards red arrows) and minima (marked by upwards yellow arrows) in the vibration energy density indicate amplitude beats of the fundamental mode. In (a), harmonic distortion of the fundamental mode (451 Hz) is visible at double (902 Hz) and triple frequencies (1353 Hz) (marked by horizontal green arrows). In (b), pitch glides of several modes, including the fundamental mode, can be distinguished.

between modal frequencies depend on the order of the nonlinearity in the system.[9] In playing conditions, identification of internal resonances in the gong's behavior is not straightforward as all modes are excited by a mallet strike. However, the variation of the amplitude of the fundamental mode sound in both vibration regimes (downwards red and upwards yellow arrows in Fig. 2) suggest that energy exchanges may take place between the fundamental mode and other modes. Modal active control will demonstrate the presence of such internal resonances in Sec. IV.

B. Theory of modal active control

Modal active control relies on a linear modal decomposition of the structure dynamics. Therefore, the nonlinear phenomena described in Sec. II A are not modelized by the approach presented hereafter.

The rationale for the modelling approach adopted goes as follows. In linear analysis, it is common to reduce the dynamics of vibrating system to p selected eigenmodes. Each eigenmode is the solution of a one-degree-of-freedom oscillator

$$\ddot{q}_i(t) + 2\xi_i\omega_i\dot{q}_i(t) + \omega_i^2 q_i(t) = f_i, \quad 1 \le i \le p, \tag{2}$$

where i refers to the eigenmode's number ($1 \le i \le p$), q_i, $\dot{q}_i$, and $\ddot{q}_i$ to its displacement, velocity, and acceleration, respectively, ξ_i and ω_i to the modal damping ratio and modal pulsation, and f_i to the modal force. Modal control is expressed in a so-called *state-space formulation*, that defines the state vector $\boldsymbol{X} = [q_1, ..., q_p, \dot{q}_1, ..., \dot{q}_p]^t$ and allows for the p equations (2) to be arranged in one single first-order differential equation

$$\dot{\boldsymbol{X}}(t) = \boldsymbol{A}\boldsymbol{X}(t) + \boldsymbol{G}w(t), \tag{3}$$

where $w(t)$ is the temporal disturbance signal and $\boldsymbol{G}$ defines the spatial distribution of the perturbation $w(t)$. Boldface terms indicate matrices and vectors, and scalar variables are shown in regular italicized fonts. Note that the output vibration of system Eq. (3), $Y(t)$, is provided with the help of sensor(s) and is related to the state-space vector $\boldsymbol{X}(t)$ by the sensor gain matrix $\boldsymbol{C}$, such that $Y(t) = \boldsymbol{C}\boldsymbol{X}(t)$.

The structure matrix $\boldsymbol{A}$ contains the p modal parameters ξ_i and ω_i. Defining the matrices $\Omega = diag(\omega_i^2)$, $\Xi = diag(\xi_i)$, and $\boldsymbol{0}_{p,p}$ as the $p \times p$ null matrix, $\boldsymbol{A}$ can be written as follows:

$$\boldsymbol{A} = \begin{bmatrix} \boldsymbol{0}_{p,p} & \boldsymbol{I}_p \\ -\Omega & -2\Xi\Omega \end{bmatrix}.$$

The p modal frequencies and damping ratios of the system are related to the $2p$ eigenvalues (or poles) of matrix $\boldsymbol{A}$, λ_i and its complex conjugate λ_i*,

$$\lambda_i = -\xi_i\omega_i + j\omega_i\sqrt{1-\xi_i^2}, \quad i \in [\![1, p]\!]. \tag{4}$$

The principal aim of modal active control is to alter the system's frequencies and damping ratios by a feedback command $u(t)$ which is added to Eq. (3). The control command introduces feedback terms that are proportional to modal displacements and velocities. It is therefore proportional to the state vector $\boldsymbol{X}$ through the control gain $\boldsymbol{K}$. The command is sent to the system with a set of actuator(s) which are characterized by the actuator gain matrix $\boldsymbol{B}$. This leads to the classical equation of a linear controlled system with a disturbance $w(t)$,

$$\begin{aligned} \dot{\boldsymbol{X}}(t) &= \boldsymbol{A}\boldsymbol{X}(t) + \boldsymbol{B}u(t) + \boldsymbol{G}w(t), \\ Y(t) &= \boldsymbol{C}\boldsymbol{X}(t), \quad u(t) = -\boldsymbol{K}\boldsymbol{X}(t). \end{aligned} \tag{5}$$

If we consider a single-input, single-output (SISO) system, $\boldsymbol{B}$ and $\boldsymbol{C}$ can be written as

$$\boldsymbol{B} = \begin{bmatrix} \boldsymbol{0}_{p,1} \\ g_a\boldsymbol{\Pi}^a \end{bmatrix}, \quad \boldsymbol{C} = \begin{bmatrix} g_s\boldsymbol{\Pi}^s & \boldsymbol{0}_{1,p} \end{bmatrix}.$$

$\boldsymbol{\Pi}^a$ and $\boldsymbol{\Pi}^s$ stand for the modal characteristics of the actuator and sensor, respectively. The gains of the actuator amplifier and sensor conditioner are designated by the terms g_a and g_s. The feedback loop introduced by the command $u(t)$ allows for modifying the system poles (corresponding to the eigenvalues of $\boldsymbol{A} - \boldsymbol{B}\boldsymbol{K}$); such a change pertains to a modification of the modal parameters ω_i and ξ_i as described by Eq. (4). The control gain $\boldsymbol{K}$ is derived from the user-defined target poles using a pole placement algorithm.[19]

The determination of the command u implies the knowledge ot the state-space vector $\boldsymbol{X}$ which is estimated by a Luenberger observer. The observer is characterized by the observer gain $\boldsymbol{L}$ that minimizes the error between the real and estimated output signals Y and $\widehat{Y}$, respectively. Gain $\boldsymbol{L}$ is also obtained by a pole placement algorithm.[19] In total, the governing equations of the entire system are then

$$\begin{aligned}\dot{\widehat{\boldsymbol{X}}}(t) &= (\boldsymbol{A}_m - \boldsymbol{B}_m\boldsymbol{K})\widehat{\boldsymbol{X}}(t) + \boldsymbol{L}(Y(t) - \widehat{Y}(t)),\\ \widehat{Y}(t) &= \boldsymbol{C}_m\widehat{\boldsymbol{X}}(t), \quad u(t) = -\boldsymbol{K}\widehat{\boldsymbol{X}}(t),\end{aligned} \tag{6}$$

where $\widehat{\boldsymbol{X}}$ is the estimate of the state-space vector $\boldsymbol{X}$ by the observer. $\boldsymbol{A}_m$, $\boldsymbol{B}_m$, $\boldsymbol{C}_m$ denote the system, the actuator, and the sensor matrices modelled in the observer, respectively. The identification of $\boldsymbol{A}_m$, $\boldsymbol{B}_m$, and $\boldsymbol{C}_m$ is derived from a rational fraction polynomial (RFP) algorithm[20] carried out on an experimental actuator/sensor frequency response function (FRF). The RFP algorithm evaluates the modal frequencies, damping ratios, and complex amplitudes $(a_i)_{1\le i\le p}$ corresponding to the product $\boldsymbol{B}_m\boldsymbol{C}_m$.[21] It is then possible to arbitrarily choose $\boldsymbol{B}_m$ and $\boldsymbol{C}_m$ such that $\boldsymbol{B}_m = [\boldsymbol{0}_{1,n} \quad |a_1| \quad \cdots \quad a_p|]^t$ and $\boldsymbol{C}_m = [\boldsymbol{0}_{1,p} \quad \mathbb{I}_{1,p}]$, which ensures that both matrices are real.[21] A global framework of the structure and the controller is shown in Fig. 3.

III. EXPERIMENTAL SET-UP

This section introduces the experimental set-up for the active control of the fundamental mode of the *xiaoluo*. First, a preliminary modal analysis of the gong is performed in order to determine the optimum location of the sensor and actuator on the instrument. Second, the system apparatus is described. Third, the identification of the observer model from RFP algorithm is presented.

A. Preliminary modal analysis

An initial modal analysis of the *xiaoluo* in free vibration was carried out as follows. The gong was placed horizontally on two foam blocks to ensure the free boundary conditions of a playing situation. The instrument was excited in its center by an automated impact hammer. A laser vibrometer, placed vertically above the instrument, measured the bending speed on a 1 cm step grid pattern of 429 points (the diameter of the gong was ∼23 cm). The hammer signal F and the vibrometer signal v were recorded simultaneously at each grid point and processed to derive the impedance function ($Z = v/F$) over the structure.

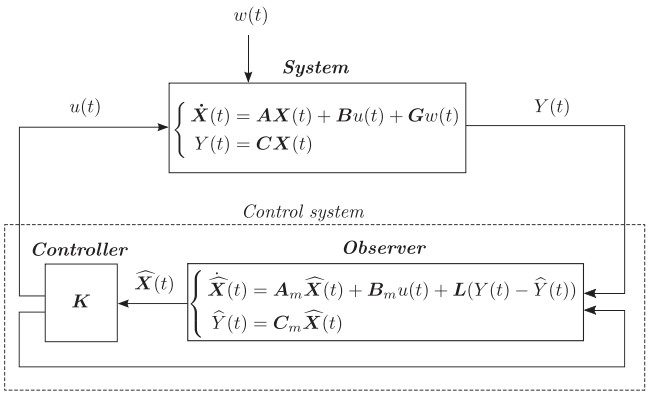

FIG. 3. Diagram of the control system.

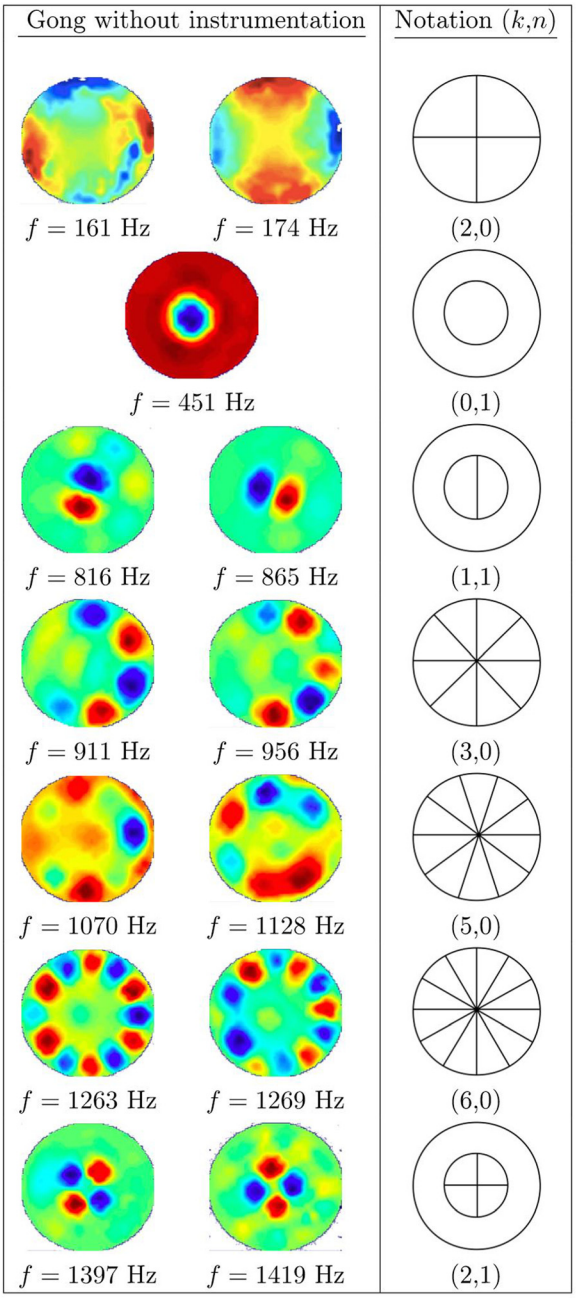

FIG. 4. (Color online) First operating deflection shapes deduced from the modal analysis of the *xiaoluo* without instrumentation. The second panel from top shows the pattern associated with the fundamental mode.

The resulting first operating deflection shapes are shown in Fig. 4 with the corresponding (k,n) notation. k and n are the number of nodal diameters and nodal circles of the deflection shapes, respectively. The fundamental mode of the instrument was ∼451 Hz and located in the central section. This analysis highlights the duplication of the asymmetric modes due to asymmetries in the geometry of the instrument. These results are consistent with the experimental modal analysis previously performed by Tsai *et al.*[22] on a *xiaoluo* and by Rossing *et al.*[12] on a *daluo*.

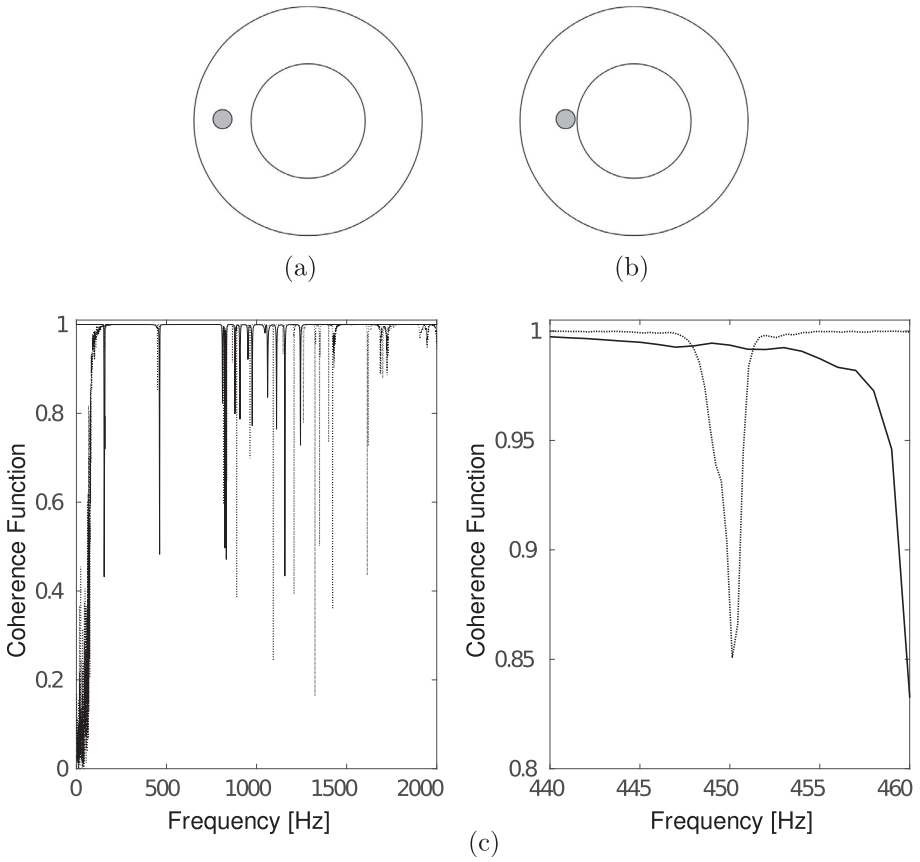

FIG. 5. (Top panels) Schematic top view of the gong showing two different locations of the actuator: (a) on the edge of the instrument and (b) close to the center. (c) Coherence function between the actuator and the sensor for an actuator positioned as in (a) (dotted line) or (b) (solid line) for the full range of frequencies (left panel) and for the frequency range around the fundamental mode (right panel).

This modal analysis allows for the identification of the location of linear modes and is therefore necessary for the location of sensor and actuator.

B. Instrumentation

Control experiments rely on an electrodynamic Tectonic Element TEAX19C01-8 actuator and a Macro Fiber Composite sensor (MFC). The MFC offers a high flexibility that allows it to be used on curved surfaces with little addition of mass and stiffness. However, it offers poor performance as an actuator, whereas the electrodynamic Tectonic Element TEAX19C01-8 actuator performs well in the frequency range of interest (100–2000 Hz). Although the modal analysis indicate that the fundamental mode is located in the center of the instrument, putting the sensor and the actuator in the central area was not feasible, because of the stiffening introduced by the instrumentation. This stiffening hinders the activation of nonlinear phenomena, whose signals stay below the measurement noise level. Therefore, the location of the sensor and actuator represents a trade-off between observing the fundamental mode and measuring weak nonlinearities (Figs. 5 and 6). The sensor and the actuator were bonded to the gong surface with thin double-sided adhesive tape. They were colocalized to improve stability of the SISO controlled system.[16]

Note that the impact of instrumentation on the vibration of the gong was evaluated by a second modal analysis. The deflection shapes exhibited by the instrumented gong are significantly similar to the ones without instrumentation (Fig. 4), highlighting a negligible impact of the instrumentation on the vibration of the structure (results are not shown in the present paper). Nevertheless, a slight change in the modal frequencies may be observed and the experimental apparatus slightly shifted the fundamental mode frequency from 451 to 449 Hz.

The COALA controller,[23] developed at IRCAM, was used for the experiments. This embedded system consists of a Beaglebone Black card running Xenomai Unix distribution. The device is equipped with a custom data acquisition cape for SISO control and allows for real-time performance with a sufficient sampling frequency; a sampling frequency of 20 kHz was used for the experiments.

The gong was held by a cord and left to hang. A mallet was suspended from a pivot system that allows for different strike angles with good reproducibility: the inter-correlation coefficient of different sensor signals obtained with the same angle strikes is above 0.95. The gong was excited either on

FIG. 6. Top view of the *xiaoluo* showing the location of the MFC sensor (left panel) and the electrodynamic actuator (right panel). The black cross shows the location of the mallet strike.

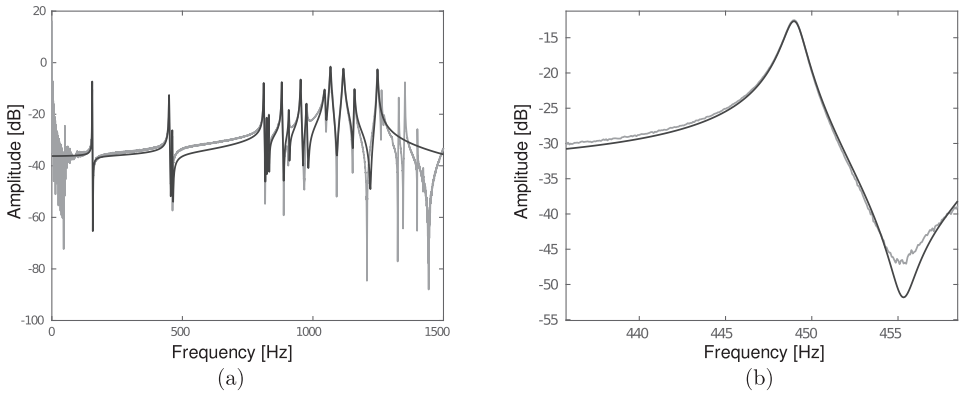

FIG. 7. Amplitude of the state-space model transfer function (black line) resulting from RFP identification of an experimental sensor-actuator FRF (shown as a grey line) for (a) the full range of frequencies and (b) the frequency range around the fundamental mode.

its circumference by the actuator with a swept sine or with the mallet at its center. However, the pitch glide regime of the gong was only achieved with a mallet strike: the position of the actuator (see Fig. 6) does not allow one to excite the large amplitude regime of the fundamental mode, located in the central area.

C. Identification and observer choices

Identification of the observer model is performed with the RFP algorithm in the range 0–1300 Hz on an experimental transfer function with a swept sine excitation (80–2000 Hz). The swept sine frequency range starts at 80 Hz as there is no mode below that frequency (see Fig. 4). The frequency range of the RFP algorithm was adjusted so that the identification is correct, equating to the quadratic error between the experimental FRF and the identified FRF being minimized.

Fifteen modes of vibration were chosen for the model, allowing for an efficient identification of the fundamental mode. This also assists in minimizing the control effects on the amplitude of high frequency modes. The amplitude of the state-space model transfer function resulting from the identification procedure is shown in Fig. 7(a), along with the experimental FRF. Note that the fundamental mode at 449 Hz is correctly identified [Fig. 7(b)]. As stated in Sec. II B, the control and observer gains $\boldsymbol{K}$ and $\boldsymbol{L}$ are calculated with a pole placement algorithm.

IV. RESULTS

In the following, the results of the damping control of the fundamental mode are introduced in two distinct steps. First, the results of the damping control in small amplitude regime (no pitch glide) are presented and the performances of modal control on the fundamental mode, harmonic distortion, and internal resonances are experimentally assessed. Second, the results of damping control in high amplitude regime (with pitch glide) are reported, and the efficiency of control system is quantified. In both cases, various damping controls ranging from -70% to $+200\%$ were applied to the fundamental mode of the gong.

A. Case of small amplitude regime

In the small amplitude regime, damping control was applied for two excitation types: (i) a swept sine (80–2000 Hz) from the actuator and (ii) a mallet strike with a small angle of about 25° (momentum $p = 31$ g m s^{-1}). The first type of excitation is classical for the observation of active control of systems; the second type of excitation allows for the observation of nonlinear phenomena.

The sensor/actuator FRFs obtained with a swept sine excitation are shown in Fig. 8 for the different control configurations. Note that the peaks widen as the damping ratio increases, as theoretically expected. The control provides a peak amplitude decrease of up to 7 dB when the damping is

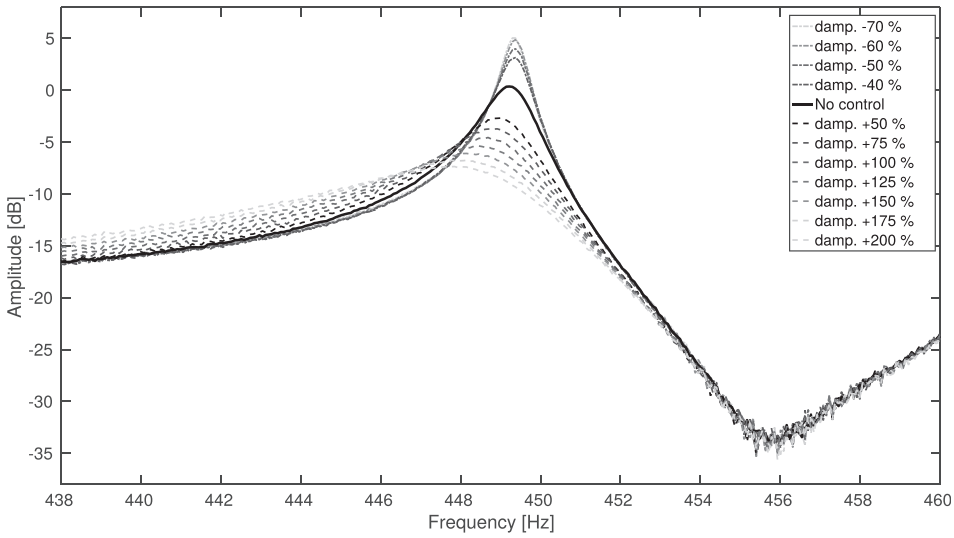

FIG. 8. Experimental sensor-actuator FRF without control and for various damping control factors.

multiplied by 3 and a peak amplitude increase of almost 5 dB when the damping is divided by 3. However, a frequency shift of about 1 Hz is observed as the damping control value increases.

Striking the gong with the mallet allows for measuring the experimental damping ratios achieved with the control, by measuring the free decay response around the fundamental mode. For this purpose, sensor signals were post-processed with a Butterworth bandpass filter, centered on the fundamental mode's frequency, and designed to have a frequency response as flat as possible in the passband. Linear regression on the slope of the resulting monochromatic signal was then performed to extract the fundamental mode damping ratio. Results are shown in Fig. 9. The difference between the target control and experimental data increases as the absolute damping control value increases while the relative error rarely exceeds 15% for larger control values.

In addition, modal control also affects frequencies other than the fundamental mode. This behavior can be observed in the fast Fourier transform (FFT) of the sensor signal (Fig. 10) for a small mallet strike with an angle of about 25° (momentum $p = 31$ g m s^{-1}). The damping control of the fundamental mode impacts other frequency components indicated by black arrows. These side effects are highlighted in Figs. 10(b)–10(d) for different control configurations. Three frequency components at 898, 1261, and 1272 Hz are controlled which exhibit a peak amplitude decrease as the fundamental mode [Figs. 11(a)–11(c)]. We will see in Sec. V that the damping control of the two latter frequencies (1261 and 1272 Hz) suggests the presence of an internal resonance between the fundamental mode and other linear modes.

B. Case of high amplitude regime

The effects of modal control on nonlinear phenomena in the small amplitude regime raises question concerning its effects in the large amplitude regime. In order to investigate this question, experiments were conducted with the same control configurations as in Sec. IV A, with strike angles ranging from 45° (momentum $p = 55$ g m s^{-1}) to 70° (momentum $p = 83$ g m s^{-1}), allowing for the observation of pitch glide. An example of damping control (+200% damping) in the large amplitude regime for a strike angle of 63° (momentum $p = 75$ g m s^{-1}) is shown in Fig. 12. The pitch glide does not appear to be affected by the control effect until it reaches a frequency close to the first mode's frequency and gets damped by the controller. Such a finding is confirmed by inspection of the sensor signals. Each of them, corresponding to a specific control configuration and strike angle, was filtered by a Butterworth bandpass filter around the frequency band of interest (400–460 Hz). This allows for observation of the controlled mode only. The envelopes of the filtered sensor signals for the different control configurations are shown in Fig. 13 for two different strike angles: 57° (momentum $p = 69$ g m s^{-1}) and 63° (momentum $p = 75$ g m s^{-1}). For each strike angle, all envelopes overlap during the first tenths of a second until a characteristic time threshold beyond which each of them decays linearly. According to Fig. 14, this time threshold seems to depend on the damping control value. This will be confirmed in Sec. V.

V. DISCUSSION

A. Assessment of control quality in the small amplitude regime

In the small amplitude regime, modal control performs well on the fundamental mode, although a frequency shift of the controlled mode is observed (Fig. 8). Such a frequency shift is larger than expected from the increase of an oscillator damping ratio. Assuming that the fundamental mode's natural frequency ω is theoretically unchanged by the control process, the associated ideal oscillatory second order model would display a monotonically decreasing value in response oscillation frequency ω' as damping ratio ξ increases, following the relation $\omega' = \omega\sqrt{1-\xi^2}$. However, since the damping ratio is identified as very small ($\xi \sim 10^{-3} \ll 1$), then we should have $\omega' \sim \omega$. It is likely that the observed shift results from imperfections in the system modelling,[24] as the phase information of the modal amplitude was not taken into account when determining the sensor and actuator

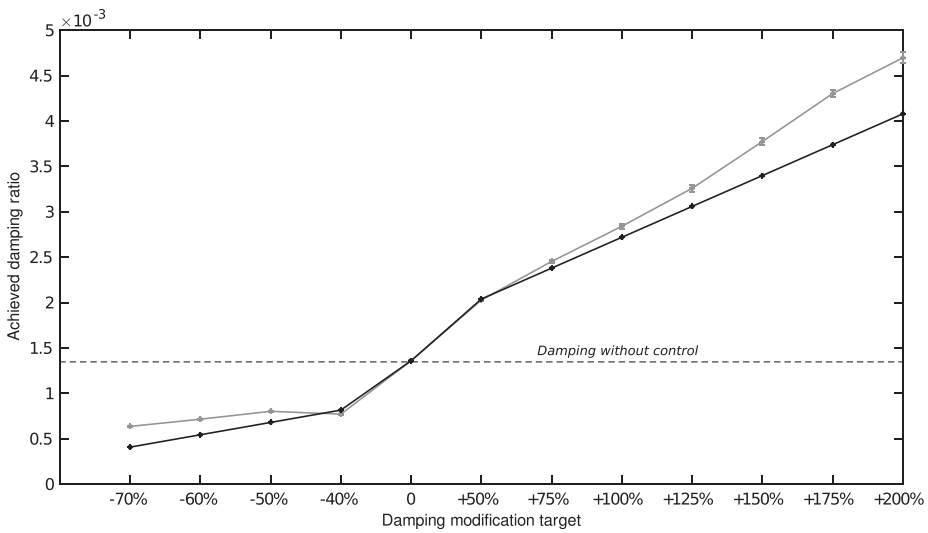

FIG. 9. Experimental damping ratios (grey line) and control target values (black line) as a function of the damping modification target (corresponding to the different control configurations). Error bars represent the residuals of the linear regression.

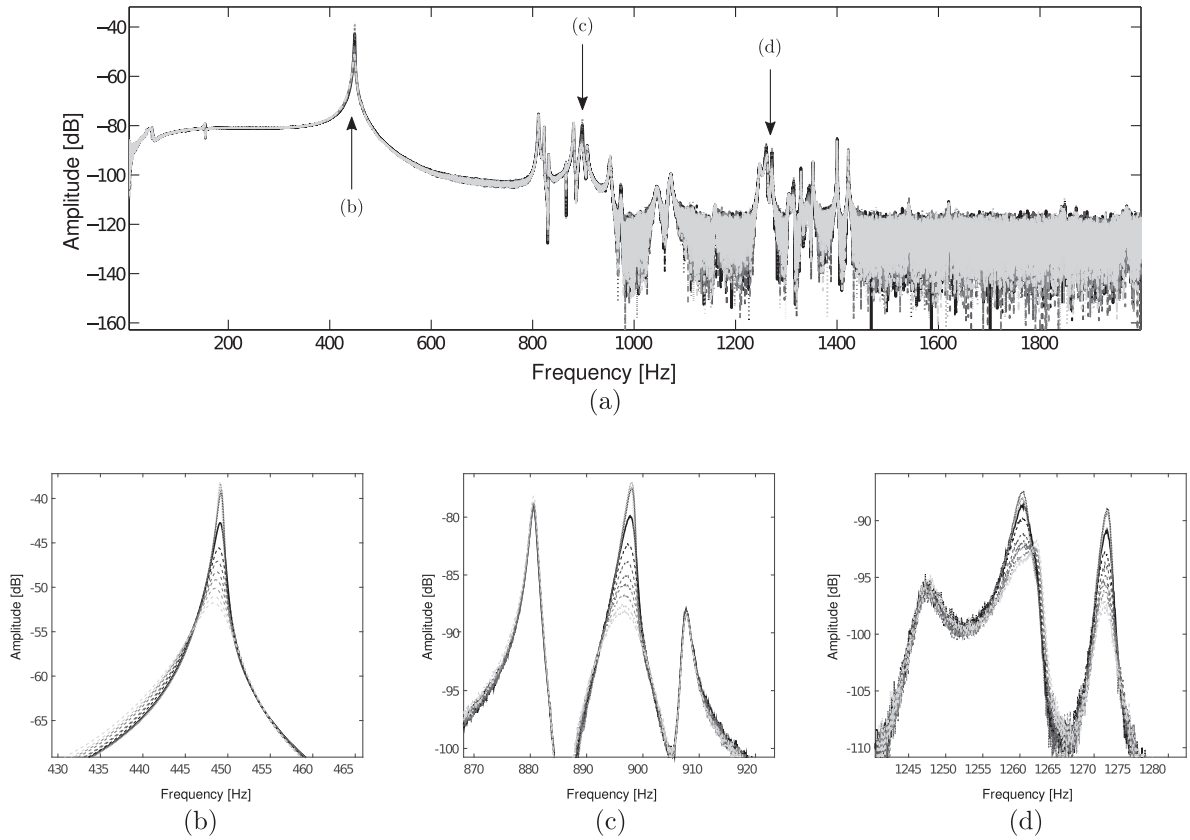

FIG. 10. FFT of the sensor signal in the damping control experiment of the fundamental mode at 449 Hz for (a) the full range of frequencies and the frequency range around (b) the fundamental mode, (c) the second order harmonic distortion (898 Hz) of this fundamental mode, and (d) the linear modes at 1261 and 1272 Hz (lines as in Fig. 8).

matrices (see Sec. II B). Such modelling imperfections could also explain the observed errors between target and experimental values (see Fig. 9).

The damping control in small amplitude regime also showed that modal control impacted nonlinear phenomena related to the controlled mode. This behavior is demonstrated in three frequency components (see Figs. 10 and 11). The first component (898 Hz) which does not correspond to a modal frequency (see Fig. 4) matches the double frequency of the fundamental mode and corresponds to the quadratic harmonic distortion. The second and third frequency components impacted by the damping control are at frequencies 1261 and 1272 Hz, and correspond to linear modes (the frequencies are not exactly the same as in Fig. 4 because of the frequency shift induced by the instrumentation). The damping variation of these latter frequency components can be understood as an 1:1:1 internal resonance phenomenon ($\omega_i + \omega_j = \omega_k$) taking place between the fundamental mode and other linear modes at 812, 823, 1261, and 1272 Hz (e.g., $449 + 812 = 1261$ and $449 + 823 = 1272$). Although such a behavior was expected, these results highlight three new features. The first concerns the control of the harmonic

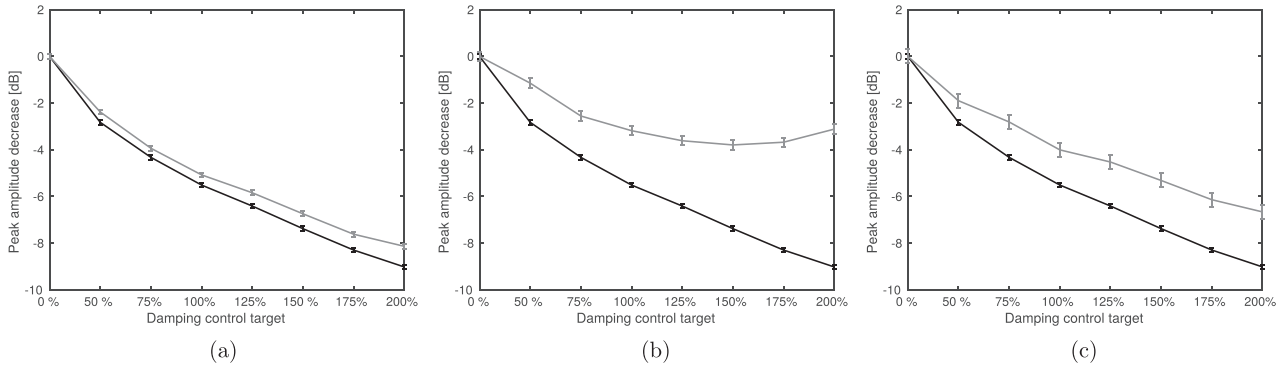

FIG. 11. Amplitude decrease of the peaks associated with frequencies impacted by the damping control experiment of the fundamental mode at 449 Hz (grey line). (a) Peak at 898 Hz, (b) peak at 1261 Hz, and (c) peak at 1272 Hz. In all panels the amplitude decrease for the fundamental mode is shown as a black line for comparison.

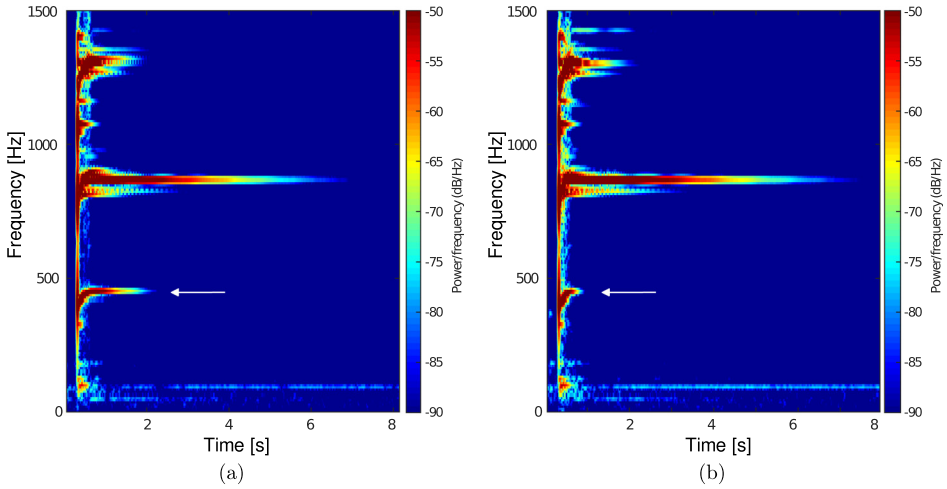

FIG. 12. (Color online) Spectrogram of the sound of the *xiaoluo* when the gong is struck with a mallet at an angle of 63° (momentum $p = 75\,\mathrm{g\ m\ s^{-1}}$) in the case (a) without control and (b) with control based on a 200% damping ratio increase of the fundamental mode at 449 Hz (located by the white arrow).

distortion which highlights the ability of modal control to impact frequency components that are *not* present in the state-space model. (Note that we have demonstrated that such impacts were not due to a spillover phenomenon.[16]) The second feature concerns the impact of modal control on internal resonances: to the author's knowledge, this is the first time that such behavior has been experimentally demonstrated. This latter result would suggest that modal control is a suitable detector of internal resonances. Moreover, our control device allowed us to detect these resonances in the free vibration regime, in contrast to earlier experimental studies[15,17] which reported detection of internal resonances

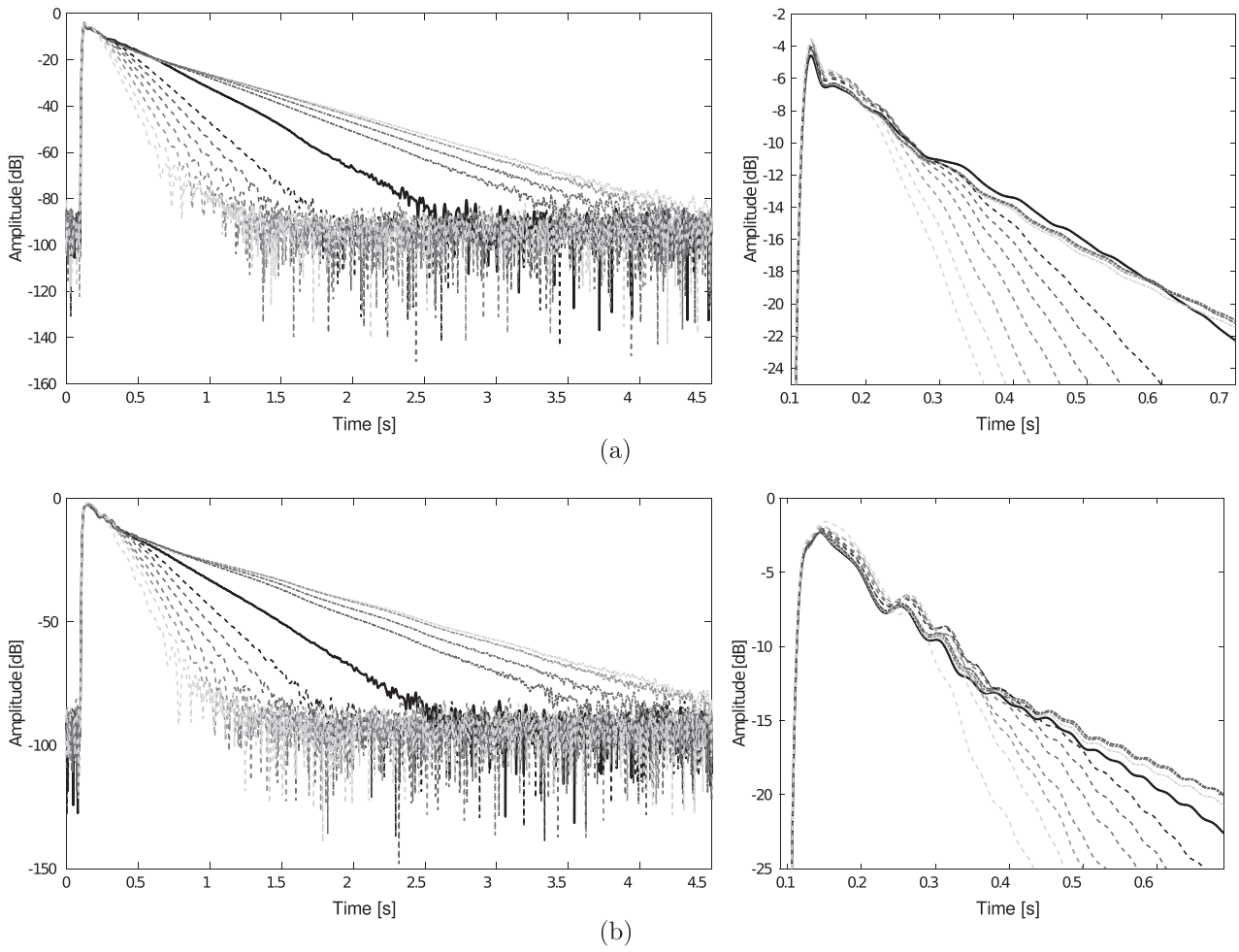

FIG. 13. Time evolution of the sensor signal envelop during the entire duration of the experiment (left panels) and for the time period around the controller trigger time (right panels) for (a) a strike angle of 57° (momentum $p = 69\,\mathrm{g\ m\ s^{-1}}$) and (b) a strike angle of 63° (momentum $p = 75\,\mathrm{g\,m\,s^{-1}}$). As in Fig. 8, different line style-color coding is used for different control configurations while the case without control is shown as a solid black line.

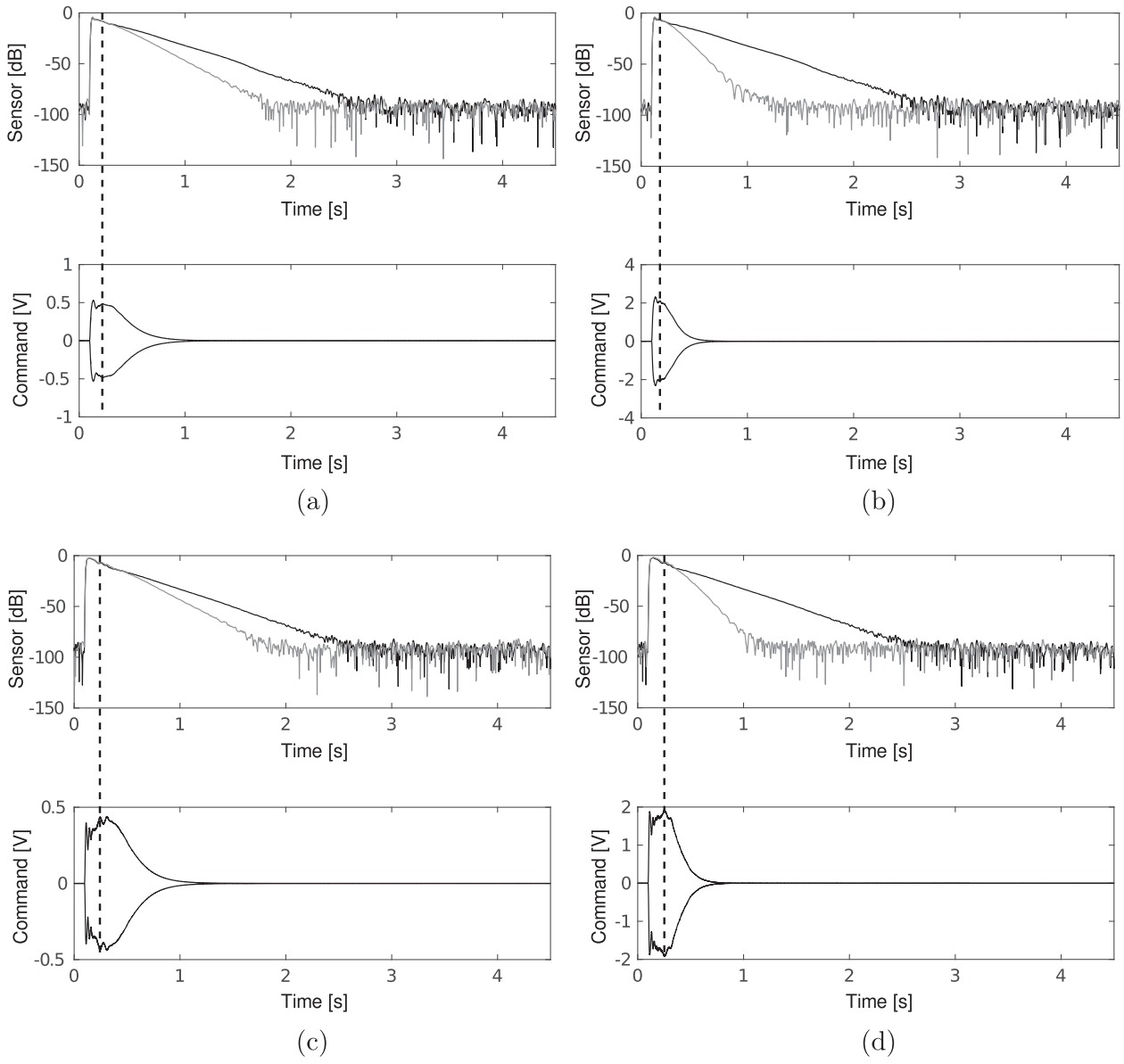

FIG. 14. Time evolution of the sensor signal envelope (top panels) and command (bottom panels), filtered in the frequency band of interest [400–460 Hz] for different control configurations: (a) damping control: +50%; strike angle: 63° (momentum $p = 75$ g m s^{-1}), (b) damping control: +150%; strike angle: 63° (momentum $p = 75$ g m s^{-1}), (c) damping control: +50%; strike angle: 46° (momentum $p = 56$ g m s^{-1}) and (d) damping control: +150%; strike angle: 46° (momentum $p = 56$ g m s^{-1}). In all panels, the case corresponding to the control configuration is shown as a grey line while the case without control is shown as a solid black line. The trigger time (shown as a vertical dashed line) corresponds to the second command maximum.

under forced stimulation. Finally, modal control on internal resonances provides useful information on energy exchange that occur between linear modes. In particular, in the case of the 1:1:1 resonances that are highlighted in Sec. IV A, the 812 and 823 Hz modes are not impacted when damping control is applied to the fundamental mode, which suggests that energy exchanges are restricted to the fundamental mode and the 1261 and 1272 Hz modes.

B. Efficiency of active modal control in large amplitude regime

The high amplitude results (Sec. IV B) underline the limits of modal control to control on pitch glide. When the system's and the observer's frequency differs significantly, the observer is not able to properly estimate the system state. However, the fact that the linear controller still has some influence on the dynamics when the frequency of the fundamental mode approaches the corresponding observer linear frequency, that is, when the signal amplitude has decreased sufficiently, is quite interesting. More precisely, one can wonder whether the trigger of the controller depends on the damping control value. This question can be investigated by looking at the relationship between the instantaneous frequency of the fundamental mode when the controller triggers and the damping control value. The controller's time trigger can be determined with the command signal. One can see on Fig. 14 that the command signal has two principal maxima: the first one corresponds to the

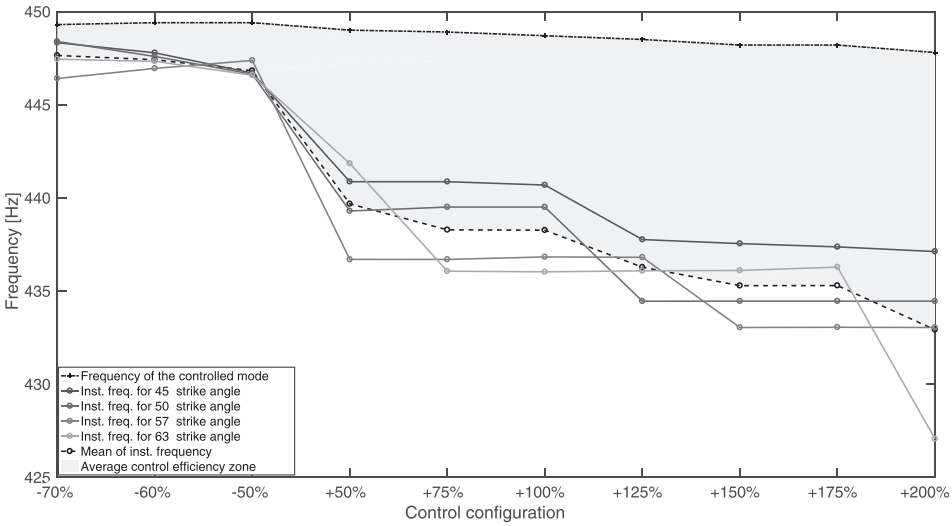

FIG. 15. Instantaneous frequency of the fundamental mode when the command is maximum, as a function of the damping control value and for different strike angles. The frequency of the fundamental controlled mode is also shown (dash-dot black line) as well as the average control efficiency zone (grey area).

impact of the mallet—since the impact is a broadband signal that causes the controller to send a command signal to all the modes. The second one is assumed to be the true trigger of the controller, that is the time when the mode is actually controlled. It is then possible to measure the instantaneous frequency of the sensor signal at this second time trigger for the different control configurations, in order to assess if the damping control value impacts the instantaneous frequency at which the control of the fundamental mode is effective. This instantaneous frequency was measured using PRAAT software for each combination of control configuration and strike angle. The results of the analysis performed for the different control configurations and four strike angles are displayed in Fig. 15. One can see that the instantaneous frequency at which the control becomes effective decreases as the damping control value increases. Moreover, this trend does not depend on the strike angle and is therefore reproducible. It is then possible to draw an average control efficiency zone (grey area in Fig. 15) corresponding to the frequency band bounded by the frequency of the controlled mode (dash-dot black line) and the mean of the trigger frequency plots of the different strike angles (dash black line). It can be assumed that the control is efficient when the observer is able to identify the instantaneous frequency of the controller identical to the one of the observer model identified by the RFP algorithm (449 Hz). In other words, the control becomes effective when the instantaneous frequency of the upward pitch glide reaches the average control efficiency zone defined above (which itself depends on the damping control value).

Finally, these considerations highlight the limited performances of the controller when dealing with frequency variations. Nonetheless, an efficient control of the pitch glide could be realized by (i) designing an adaptive linear observer whose matrix A varies at the same time as the instantaneous frequency of the fundamental mode, or (ii) creating a nonlinear observer including a nonlinear model of the gong. This latter solution would significantly benefit from the work of Touzé[25] on nonlinear normal modes[26] applied to plates and shells.

VI. CONCLUSION

An experimental protocol was developed in order to carry out the modal control of a gong with geometric nonlinearities. A modal analysis of the structure and an identification process led to the implementation of a SISO control system manipulating the damping of the fundamental mode.

In the small amplitude regime, experimental damping control of the fundamental mode provides good experimental results. Additionally, results demonstrate that the damping control acts both on the controlled mode and on the frequencies involved in nonlinear phenomena such as distortion and internal resonances. The control of harmonic distortion highlights the ability of modal control to affect frequency components initially absent from the linear state-space model of the observer. On the other hand, the effects of modal control on internal resonances is demonstrated for the first time, opening up new perspectives for their detection and comprehension.

The study also underlines the limited performances of the modal control regarding the control of the fundamental pitch glide which are mainly due to the difference between the system instantaneous frequency, gliding upward, and the frequency identified by the RFP algorithm in the observer model (449 Hz). These limitations were quantified by measuring the instantaneous frequency band around the controlled mode that allows for an efficient damping control. The control setup was found to be efficient once the instantaneous frequency of the controlled mode reaches an average frequency band which depends on the damping control value.

In total, a global control of the pitch glide may require additional modelling of the nonlinear dynamics of the *xiaoluo*. This work represents a first step towards the control of nonlinear musical instruments. Future work deriving from this study could aim to implement a completely configurable gong for musical practice and composition.

ACKNOWLEDGMENTS

This work was funded by the Université Pierre et Marie Curie (France). The authors would like to especially thank

Camille Dianoux, Arnaud Récher, and Alain Terrier for their major support with the elaboration of the experimental set up, as well as Robert Piéchaud for his help with the COALA system.

[1]S. Hanagud and S. Griffin, "Active structural control for a smart guitar," in *Fourth European Conference on Smart Structures and Materials* (1998), pp. 169–175.
[2]T. Meurisse, A. Mamou-Mani, R. Caussé, and D. Sharp, "An active mute for the trombone," J. Acoust. Soc. Am. **138**, 3539–3548 (2015).
[3]H. Wright, "The acoustics and psychoacoustics of the guitar," Ph.D. thesis, University of Wales, College of Cardiff (1996).
[4]N. Fletcher and T. Rossing, *The Physics of Musical Instruments* (Springer-Verlag, London, 1998), pp. 673–679.
[5]S. Benacchio, B. Chomette, A. Mamou-Mani, and V. Finel, "Mode tuning of a simplified string instrument using time-dimensionless state-derivative control," J. Sound Vib. **334**, 178–189 (2015).
[6]S. Benacchio, A. Mamou-Mani, B. Chomette, and V. Finel, "Active control and sound synthesis-two different ways to investigate the influence of the modal parameters of a guitar on its sound," J. Acoust. Soc. Am. **139**, 1411–1419 (2016).
[7]T. Meurisse, A. Mamou-Mani, S. Benacchio, B. Chomette, V. Finel, D. B. Sharp, and R. Caussé, "Experimental demonstration of the modification of the resonances of a simplified self-sustained wind instrument through modal active control," Acta Acustica **101**(3), 581–593 (2015).
[8]O. Thomas, C. Touzé, and A. Chaigne, "Nonlinear behavior of gongs through the dynamics of simple rods systems," in *Proceedings of the International Symposium on Musical Acoustics 1*, Perugia, Italy (September 10–14, 2001), pp. 179–178.
[9]A. H. Nayfeh and D. T. Mook, *Nonlinear Oscillations* (Wiley-VCH, Weinheim, 1995), pp. 1–720.
[10]A. Chaigne, C. Touzé, and O. Thomas, "Nonlinear vibrations and chaos in gongs and cymbals," Acoust. Sci. Technol. **26**(5), 403–409 (2005).
[11]K. Legge and N. Fletcher, "Nonlinearity, chaos, and the sound of shallow gongs," J. Acoust. Soc. Am. **86**(6), 2439–2443 (1989).
[12]T. D. Rossing and N. Fletcher, "Nonlinear vibrations in plates and gongs," J. Acoust. Soc. Am. **73**(1), 345–351 (1983).
[13]N. Fletcher, "Nonlinear frequency shifts in quasispherical-cap shells: Pitch glide in Chinese gongs," J. Acoust. Soc. Am. **78**(6), 2069–2073 (1985).
[14]G. Kerschen, K. Worden, A. F. Vakakis, and J-C. Golinvaltitle, "Past, present and future of nonlinear system identification in structural dynamics," Mech. Syst. Sign. Process. **20**(3), 505–592 (2006).
[15]M. Monteil, O. Thomas, and C. Touzé, "Identification of mode couplings in nonlinear vibrations of the steelpan," Appl. Acoust. **89**, 1–15 (2015).
[16]A. Preumont, *Vibration Control of Active Structures: An Introduction*, 3rd ed. (Springer Science & Business Media, Berlin, 2012), Vol. 50, pp. 1–80.
[17]O. Thomas, C. Touzé, and A. Chaigne, "Non-linear vibrations of free-edge thin spherical shells: Modal interaction rules and 1: 1: 2 internal resonance," Int. J. Solids Struct. **42**(11), 3339–3373 (2005).
[18]A. H. Nayfeh and W. Lacarbonara, "On the discretization of distributed-parameter systems with quadratic and cubic nonlinearities," Nonl. Dynam. **13**(3), 203–220 (1997).
[19]J. Kautsky, N. K. Nichols, and P. Van Dooren, "Robust pole assignment in linear state feedback," Int. J. Control **41**(5), 1129–1155 (1985).
[20]M. H. Richardson and D. L. Formenti, "Parameter estimation from frequency response measurements using rational fraction polynomials," in *Proceedings of the International Modal Analysis Conference*, Orlando (1982), pp. 167–182.
[21]S. Chesne, C. Jean-Mistral, and L. Gaudiller, "Experimental identification of smart material coupling effects in composite structures," Smart Mater. Struct. **22**(7), 075007 (2013).
[22]G.-C. Tsai, B.-T. Wang, Y.-S. Lee, and Z.-W. Chang, "Study of vibration and sound characteristics of a copper gong," J. Chin. Inst. Eng. **28**(4), 713–719 (2005).
[23]R. Piéchaud, "A lightweight C++ framework for real time active control," *16th Real Time Linux Workshop* (Düsseldorf, 2014).
[24]B. Chomette, D. Remond, S. Chesne, and L. Gaudiller, "Semi-adaptive modal control of on-board electronic boards using an identification method," Smart Mater. Struct. **17**(6), 065019 (2008).
[25]C. Touzé, O. Thomas, and A. Chaigne, "Hardening/softening behaviour in non-linear oscillations of structural systems using non-linear normal modes," J. Sound Vib. **273**(1-2), 77–101 (2004).
[26]G. Kerschen, M. Peeters, J. C. Golinval, and A. F. Vakakis, "Nonlinear normal modes, Part I: A useful framework for the structural dynamicist," Mech. Syst. Sign. Process. **23**(1), 170–194 (2009).